Relating State-Dependent Cross Sections to Non-Arrhenius Behavior for the Cl + CH_4 Reaction†

Hope A. Michelsen*

Combustion Research Facility, Sandia National Laboratories, MS 9055, P.O. Box 969, Livermore, California 94551

William R. Simpson

Department of Chemistry, University of Alaska, Fairbanks, Alaska 99775

Received: May 3, 2000; In Final Form: August 7, 2000

We have used information gained via differential cross-section experiments of the Cl + CH_4 reaction in an analysis of measured thermal rate constants to determine the source of the observed non-Arrhenius behavior. Our results demonstrate that curvature in the Arrhenius plot at temperatures above room temperature can be explained by enhancement of the reaction rate when the symmetric or asymmetric stretch of CH_4 is excited. At low temperatures, the apparent curvature can be explained by tunneling and modest reaction-rate enhancement by a low-frequency bending mode of CH_4. An analysis of dynamical and thermal measurements of the kinetic isotope effect for Cl + CH_4/CD_4 indicates that tunneling enhances the reaction probability of hydrogen-atom abstraction by partially relaxing the steric restrictions for the collinear geometry of the transition state. This analysis provides an estimate of rate constants at low (atmospheric) temperatures that is higher than recommended values and provides a prediction of rate constants at high (combustion) temperatures for which measurements are not currently available. We suggest directions for future theoretical and experimental studies based on uncertainties in the current description of this important reaction.

Introduction

Thermal rate constants have been used extensively to extract information about mechanisms for simple chemical reactions.[1] The importance of the reaction of atomic chlorine with methane,

$$Cl + CH_4 \rightarrow CH_3 + HCl$$

in atmospheric and combustion chemistry has prompted a large number of studies of the rate constants for this reaction, collectively spanning the temperature range of 180−800 K.[2−25] These studies have shown that this endothermic reaction has an activation energy (∼900 cm^{-1}) not much larger than the heat of reaction (600 cm^{-1}) and a preexponential factor (10^{-11} cm^3 $molecule^{-1}$ s^{-1}) significantly smaller than the hard-sphere collision rate (3×10^{-10} cm^3 $molecule^{-1}$ s^{-1} at room temperature).

In the early 1960s, Johnston and co-workers[26,27] performed pioneering studies relating kinetic data to features of the potential energy surfaces (PESs) for this and other photochlorination reactions. Their work demonstrated that activated-complex theory (also known as transition-state theory) could be used to predict rate constants for bimolecular gas-phase reactions, such as Cl + CH_4, as long as neither the activation energy nor the temperature is too low. With the advent of faster computers, calculations have been extended to multidimensional simulations on more detailed PESs.[28−39] These advances have not resulted in predictive capabilities significantly better than those provided by relatively simple transition-state theory for thermal rate constants at moderate temperatures, but have led to more accurate calculations at low temperatures.

Despite extensive theoretical and experimental investigations of Cl + CH_4, however, the rate constants for this reaction are uncertain at low (stratospheric) and high (combustion) temperatures, where kinetic measurements are difficult. This reaction has been implicated in the initiation of soot formation during the combustion of CH_4 in the presence of chlorine or chlorinated hydrocarbons.[40,41] Measurements are only available for temperatures as high as 800 K,[24] however, far below the 1500−2500 K desirable for combustion modeling. At stratospheric temperatures, on the other hand, rate constants have been measured by several groups,[4−6,11,13,14,17,18,20−23] yielding results that differ by as much as a factor of 2 in the range of 215−220 K.[5,6,13,14,18,20−22] Even a difference of 27% at these temperatures has been shown to have a substantial effect on the calculated abundance of stratospheric HCl.[42] Furthermore, this reaction exhibits significant non-Arrhenius behavior (deviations from a simple exponential dependence on inverse temperature), making extrapolation from moderate temperatures to these more extreme temperatures unreliable.

Non-Arrhenius behavior is common and can be attributed to a variety of factors. For the Cl + CH_4 reaction, a number of studies have indicated that tunneling contributes to the curvature in the Arrhenius plot at low temperatures.[14,22,31,33,36] Heneghan et al.[11] showed that the estimated temperature dependence of the transition-state heat capacity can lead to curvature at high temperatures. Ravishankara and Wine[23] hypothesized that the non-Arrhenius behavior and the large variability in the low-temperature measurements could be attributable to differential reactivity of thermally accessible electronic states of Cl. The electronic quenching rates on which their analysis was based have since been demonstrated to be inaccurate, however, and

† Part of the special issue "Harold Johnston Festschrift".

10.1021/jp0016784 CCC: $20.00
Published on Web 11/30/2000

recent studies have indicated that the reaction of CH_4 with electronically excited Cl is not significantly faster than with the ground state of Cl.[25,43,44]

Kandel and Zare[44] alternatively suggested that the non-Arrhenius behavior could result from differential reactivity of the vibrational states of CH_4. Simpson et al.[45,46] recently measured the relative state-dependent reaction cross sections for the Cl + CH_4 reaction and demonstrated that exciting CH_4 in the asymmetric stretch (υ_3) enhances the reaction probability by a factor of 30. In addition, Kandel and Zare[44] hypothesized that vibrational energy in the umbrella (υ_4) or torsional (υ_2) bending modes of CH_4 may also enhance reactivity. These latter studies indicate that CH_4 with energy in the umbrella and torsional modes may be more reactive than CH_4 with energy in the stretch mode. Earlier work by Hsu and Manuccia[47−49] suggested that exciting the CH_2 rocking mode (υ_7) of CH_2D_2 significantly enhances the reaction rate, whereas experiments by Vijin et al.[50] and Chesnokov et al.[51] indicated that neither pumping the umbrella mode of CD_4 nor exciting the umbrella or torsional modes of CH_4 enhances the reaction rate significantly. Vibrational enhancement of the reaction probability is indicative of a late barrier along the reaction coordinate on the PES, for which the transition state resembles the products more than the reactants. A late barrier is consistent with measurements of the product rotational alignment.[52]

Theoretical calculations by Duncan and Truong,[31] Yu and Nyman,[37] and Corchado et al.[38] also support observations of vibrational enhancement, although the calculations suggest that energy in the symmetric stretch (υ_1) should be far more effective at promoting the reaction than energy in the umbrella bend mode and that energy in the torsional mode is unlikely to be effective. Calculations indicate that the transition state is highly collinear,[28−31,34] which is consistent with observations of a predominantly backscattered angular distribution for the HCl product (with respect to the direction of approach of Cl),[45,46,53] forward-scattered angular distribution for the CH_3 product,[44] and rotationally cold internal state distributions for HCl and CH_3.[44−46,53] Vibrational energy appears to increase the reaction probability by opening the cone of acceptance of the transition state, thereby partially lifting the steric restrictions for surmounting the barrier to reaction.[45,46]

This paper presents a framework in which the dynamical information provided by the experiments of Zare and co-workers[44−46] can be combined with the vast body of kinetic data to construct a description of this reaction that can be used in atmospheric and combustion modeling applications. Our goal is to make use of disparate experimental results to provide greater confidence in the low-temperature rate constants used in atmospheric modeling studies and in the prediction of high-temperature rate constants used in combustion modeling studies.

In general, if the reaction probability for a reaction with an activation barrier has been measured in sufficient detail as a function of translational, vibrational, and rotational energy, these data can be used to calculate thermal rate constants. State-dependent measurements at collision energies that are low enough to allow such an analysis are rare. The Maxwell speed distribution is centered at collision energies well below the reaction barrier for most activated reactions. Understanding how the reactivity can be enhanced at these collision energies by vibrational and rotational motion is thus critical to being able to derive a thermal rate constant. State-dependent measurements using molecular beams or initiated by photolytic production of a "hot atom" (i.e., nonthermalized) reagent, however, are generally restricted to collision energies close to or above the barrier height. To date, there are no activated gas-phase reactions for which the energetics have been determined well enough to derive thermal rate constants, and such an analysis has only been accomplished for one gas−surface reaction.[54,55]

The barrier estimated for the Cl + CH_4 reaction is low (1200−1700 cm^{-1}),[28−38] and state-dependent cross section measurements are only available for collision energies (1050−2280 cm^{-1}) close to the barrier height and above.[44−46] These collision energies are significantly higher than the activation energy (~900 cm^{-1}). Nevertheless, we have used the information gained from these measurements, combined with an analysis of the thermal rate constants measured for this reaction, to investigate the source of the observed non-Arrhenius behavior. Using the results of this analysis, we predict rate constants for higher temperatures and derive a more reliable estimate for rate constants at lower temperatures.

We have extended this analysis to measurements of the H/D kinetic isotope effect (KIE) for Cl + CH_4/CD_4. As a test of transition-state theory, Johnston and co-workers[27] made the first measurements of the KIE for the Cl + CH_4/CD_4 and other photochlorination reactions. They concluded that the activated-complex model predicts qualitative trends without reproducing the magnitude of the KIE observed. More recent theoretical calculations have been compared with these experimental values and have demonstrated marginal agreement in one case[33] and significantly better agreement in others.[34,38] Our analysis of the KIE suggests that tunneling effectively opens the cone of acceptance for H atom transfer, which could contribute to the observed non-Arrhenius behavior.

Experimental Section

Thermal Rate Constants. Thermal rate constants for the title reaction have been measured many times over the past several decades.[2−25] Figure 1 summarizes the results of these experiments. Although experimental details vary from study to study, the techniques used to make these measurements can be grouped into general categories defined by the method of production of reactant Cl radicals and the method of detection of products or reactants. In each of these studies, atomic chlorine was produced by dissociation of a chlorinated species (e.g., Cl_2, CCl_4, CCl_2F_2, $CClF_3$, $C_2Cl_3F_3$, HCl) by microwave discharge,[6−18] UV photolysis,[3−6,19−25] or thermal neutrons.[2] Loss of Cl was monitored by resonance fluorescence,[13−23] laser-induced fluorescence,[25] or mass spectrometry.[6−12] Alternatively, product formation was measured by IR absorption spectroscopy[24] or mass spectrometry.[8−12]

Several studies provided rate constants for Cl + CH_4 referenced to rate constants for another reaction rather than absolute rate constants for either reaction.[2−6] These competitive chlorination experiments employed detection techniques such as UV−vis or IR absorption spectroscopy,[5] gas chromatography,[4,6] or fractional distillation[3] to determine relative concentrations of products. Previous compilations of rate constants for this reaction have demonstrated that the rate constants inferred from competitive chlorination experiments are systematically lower than the absolute rate constant measurements.[56,57] Figure 2 shows measured rate constants for two reference reactions used to infer the rate constants for Cl + CH_4. Most of the measurements fall above the recommended values (dashed lines) in the relevant temperature range (198−630 K for Cl + C_2H_6,[16,19,21,24,58−62] 197 and 217 K for Cl + O_3[63−69]). To derive the rate constants for Cl + CH_4 from the experiments that used Cl + C_2H_6 as a reference reaction,[2−4,6] we used the results of a weighted nonlinear least-squares fit to the measured rate

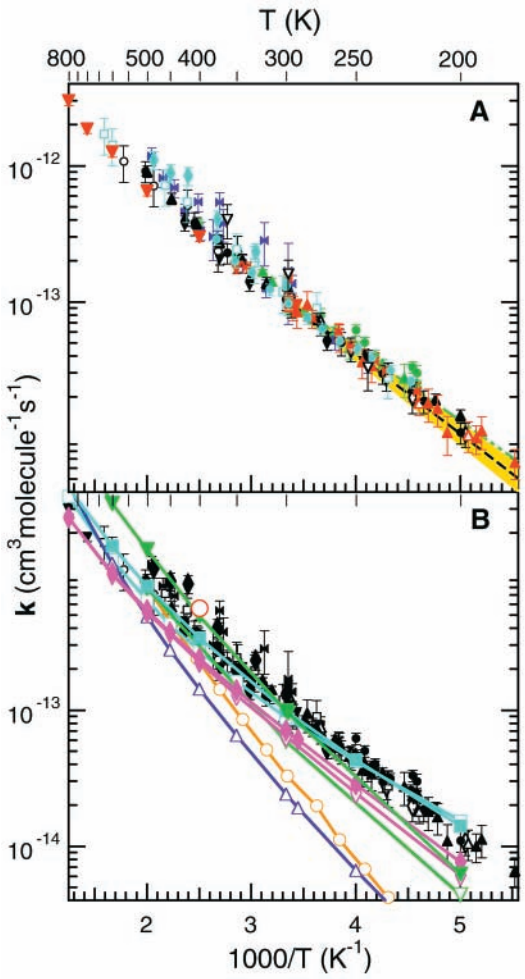

Figure 1. Arrhenius (semilogarithmic) plot of measured and calculated rate constants for Cl + CH_4 → CH_3 + HCl. Rate constants are shown as a function of inverse temperature. Measured values include those of (▽) Lee and Rowland,[2] (○) Pritchard et al.,[3] (blue □) Knox and Nelson,[4] (red △) DeMore,[5] (◇◆) Lin et al.,[6] (blue ♦) Clyne and Walker,[7] (purple ⋈) Poulet et al.,[8] (red ♦) Sawersyn et al.,[9] (red ×) Baghal-Vayjooee et al.,[10] (red ⋈) Heneghan et al.,[11] (red ●) Dobis and Benson,[12] (purple ■) Keyser,[13] (●) Zahniser et al.,[14] (blue ▼) Michael and Lee,[15] (green ◆) Beichert et al.,[16] (red ▲) Seeley et al.,[17] (red *) Wang and Keyser,[18] (red ■) Davis et al.,[19] (green ●) Watson et al.,[20] (green ▲) Manning and Kurylo,[21] (▲) Whytock et al.,[22] (blue ●) Ravishankara and Wine,[23] (red ▼) Pilgrim et el.,[24] and (red +) Matsumi et al.[25] Open symbols indicate rates inferred from competitive chlorination measurements relative to rates derived from the measurements shown in Figure 2 (see text). (A) Lines represent rates recommended by Sander et al.[56] (dashed black with estimated 1σ uncertainties represented by yellow shading) and Atkinson et al.[57] (dot−dashed green). (B) Measured rate constants (black symbols) are compared with the results of theoretical calculations from Johnston and Goldfinger[26] (open red circle), Gonzalez-Lafont et al.[29] (green line with solid inverted triangles), Dobbs and Dixon[30] (orange line with open circles), Duncan and Truong[31] (purple line with open triangles), Espinosa-García and Corchado[33] (cyan line with open squares), Roberto-Neto et al.[34] (green line with inverted open triangles), Nyman et al.[35] (magenta line with solid diamonds), Yu and Nyman[36] (magenta line with open diamonds), and Corchado et al.[38] (cyan line with solid squares).

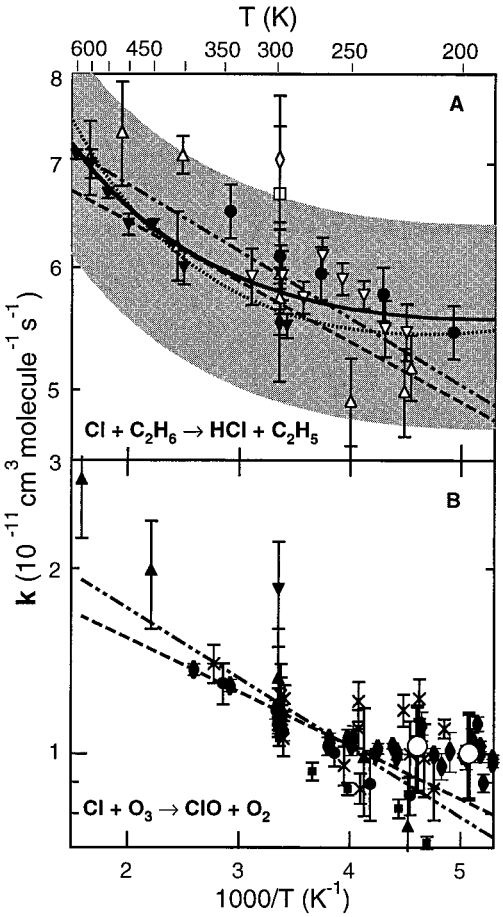

Figure 2. Arrhenius (semilogarithmic) plot of measured rate constants for reference reactions used in competitive chlorination experiments. Rate constants are shown as a function of inverse temperature. (A) Measured values for Cl + C_2H_6 → C_2H_5 + HCl from (□) Davis et al.,[19] (▽) Manning and Kurylo,[21] (△) Lewis et al.,[58] (×) Ray et al.,[59] (●) Dobis and Benson,[60] (◇) Kaiser et al.,[61] (+) Stickel et al.,[62] (◆) Beichert et al.,[16] and (▼) Pilgrim et el.[24] The dashed line is the value recommended by Sander et al.,[56] the dot dashed line is the recommended value from Atkinson et al.,[57] the dotted line is the fit given by Pilgrim et al.,[24] and the thick solid line is a nonlinear least-squares fit to the data weighted by the 1σ total uncertainty shown, $k(T) = 4.21 \times 10^{-11}$-$(T/298)^{0.492}$ exp(94.85/T) molecules cm^{-3} s^{-1}. The shaded region represents ±15% from the fit. (B) Measured valued for Cl + O_3 → ClO + O_2 from (▲) Clyne and Watson,[63] (▼) Clyne and Nip,[64] (■) Kurylo and Braun,[65] (●) Watson et al.,[66] (*) Zahniser et al.,[67] (♦) Nicovich et al.,[68] (×) Seeley et al.[69] The dashed line is the value recommended by Sander et al.,[56] and the dot dashed line is the recommended value from Atkinson et al.[70] The open circles are the average values from rate constants measured at 197 and 217 ± 3 K with error bars representing the 1σ standard deviation of the weighted mean of data points at 217 ± 3 K.

constants (Figure 2a). (The parameters derived from this fit are given in the caption of Figure 2a.) For the experiment that used Cl + O_3 as a reference,[5] we averaged the data at the two relevant temperatures with error bars derived from the scatter of the data at 217 K. The resulting rate constants shown in Figure 1 are generally consistent within 1σ with the absolute rate constant measurements for Cl + CH_4; i.e., this analysis reconciles the differences between the competitive chlorination data and the absolute rate constant measurements.

Figure 1a also presents values recommended for use in atmospheric models.[56,57] These recommendations were derived from unweighted fits of a standard Arrhenius expression to multiple data sets. There are considerable differences between values recommended by the NASA panel[56] and the IUPAC committee.[57] Although the uncertainties estimated for the NASA recommendations[56] encompass most of the data, the measurements tend to be higher than the recommended values at low temperatures (below 260 K, 80% of all measured rate constants are higher than values recommended by Sander et al.;[56] the average difference between 180 and 260 K is 14%). The recommendations provided by the IUPAC committee[57] are also

higher than the NASA recommendations[56] by more than the 1σ uncertainties of the NASA values. Recommendations derived from multiple data sets are not available for temperatures above 300 K. At these temperatures, the data are relatively sparse, and the scatter in the available measurements is large. Nevertheless, significant deviations from simple Arrhenius behavior have been noted previously for this temperature regime.[13,14,20,24] At lower temperatures non-Arrhenius behavior has also been noted.[13,14,22,23]

The degree of curvature and effective activation energy measured over the temperature range of 200−800 K are generally not reproduced in theoretical studies. Figure 1b shows a comparison of the results of several theoretical investigations[26,29−31,33−36,38] with the measured rate constants. Agreement tends to be better at the higher end of this temperature range. Tunneling effects are expected to be less significant at these higher temperatures, suggesting that the disagreement at lower temperatures may be attributable to the semiclassical tunneling approximations employed.[30,31,34,36] In addition, discrepancies between measured and calculated rate constants may be related to limitations of the PESs on which these calculations were based[30,31,34,36] or unaccounted for spin−orbit coupling effects.[36] Espinosa-García and Corchado[33] used experimentally determined reactant and product molecular constants to constrain the PES in the entrance and exit channels. Corchado et al.[38] additionally constrained the PES using the mean value of the room-temperature measurements of the rate constant for Cl + CH_4. Their results demonstrate the best agreement with the measurements. Even for these calculations, however, the results are not sufficiently accurate to resolve the discrepancies in measured values at low temperatures or to predict rate constants for higher temperatures.

Differential Reaction Cross Sections. Theoretical studies have suggested that the transition state for the ground-state reaction of Cl with CH_4 is highly collinear along the C−H−Cl axis.[28−31,34] These results are supported by experimental investigations, which have shown that, for the ground-state reaction, the angular distribution of the HCl product is predominantly backscattered,[45,46,53] the angular distribution of the CH_3 product is predominantly forward scattered,[44] and the internal state distributions for these products are rotationally cold.[44−46,53] Experiments by Simpson et al.[45,46] have demonstrated that exciting the asymmetric stretch of CH_4 enhances its reactivity with Cl. In these experiments, Simpson et al.[45,46,71] measured the internal state-specific angular distribution of the HCl product of the ground-state reaction and repeated the experiment using an IR laser to excite the asymmetric CH stretch of CH_4. The results showed that placing one quantum of vibrational energy in the asymmetric stretch leads to a forward- and backward-scattered HCl($v = 1$) product and a backward- and side-scattered HCl($v = 0$) product with more rotational energy than observed for the ground-state reaction. These results imply that vibrational excitation of the CH stretch lifts the tight steric restrictions of the collinear transition state and opens the cone of acceptance for reaction.[45,46] Kandel and Zare[44] probed the CH_3 instead of the HCl product for the ground-state reaction and observed products with more translational energy than could be accounted for by the energetics of the reaction. They hypothesized that these results could be explained by reactions involving low-frequency bending modes of CH_4 and have suggested that excitation of the umbrella or torsional modes of CH_4 also enhances reactivity of CH_4 with Cl. More side-scattered CH_3 product was observed from the reaction they associated with CH_4 in one of these bending modes than for reaction with ground-state CH_4, which suggests that the bending mode also relaxes the collinear requirement for the transition state.[44]

The results of the experiments by Simpson et al.[45,46] indicate that the reaction probability is enhanced over that of the ground-state reaction by a factor of ~30 for a collision energy of 1274 cm^{-1} when the asymmetric stretch is excited. Further studies of the ground-state reaction by Kandel and Zare[44] demonstrated excess product translational energy, which Kandel and Zare speculated resulted from reactions involving excited CH_4 bending modes. With this interpretation of their results, they estimated that the reaction probability is enhanced by factors within an order of magnitude of 400 for a collision energy of 1040 cm^{-1} and 200 for a collision energy of 1961 cm^{-1} when a bending mode is excited.[44] (Because the reactant states were thermally populated, distinguishing between contributions from the umbrella and torsional modes was not possible in this experiment.) These results indicate that the bending mode may be more effective at promoting the reaction than is the asymmetric stretch at collision energies near 1300 cm^{-1}. For a reaction with a late barrier, a collinear transition state, and a planar geometry for the methyl product,[72] it is not surprising for both the stretch and umbrella bend to enhance the reaction probability.[73] Vibrational enhancement of the reaction probability for this reaction is supported by recent transition-state theory and quantum-scattering calculations.[31,35,37,38] In contrast to the experimental results, however, these calculations predict that excitation of the stretch should be much more effective than that of the umbrella or torsional bend in promoting reactivity,[31] as might be expected given the relatively large energy of a vibrational quantum of the stretch compared to that of the bend.

Kinetic Isotope Effect. Relatively few experiments have been performed to measure the KIE for the Cl + CH_4 reaction.[7,25,27,50,74−79] Figure 3 summarizes the KIE measurements for Cl + CH_4/CD_4.[7,25,27,50,75] At all temperatures, the Cl + CH_4/CD_4 rate constant ratio is >1.

The observed KIE may be attributable to differences in the zero-point energies (ZPE) of the reactants. The ZPE for CD_4 is ~2496 cm^{-1} lower than that for CH_4. The calculations of Roberto-Neto et al.[34] predict that the transition-state ZPE for $ClDCD_3$ is ~2876 cm^{-1} lower than that for $ClHCH_3$, suggesting that the effective barrier is lower (by ~380 cm^{-1}) for CD_4 than for CH_4 and indicating that the direction of the KIE should be opposite to that observed. If we consider the ZPE factor only for the symmetric stretch, the normal mode that couples most strongly to the reaction coordinate, however, the effective barrier should be higher for abstraction of deuterium over hydrogen by ~310 cm^{-1}, based on calculated frequencies for the transition state from Roberto-Neto et al.[34] The trend in KIE is thus qualitatively consistent with the measured values if energy placed in the stretching mode is much more effective than other modes in surmounting the reaction barrier.

On the other hand, the frequencies of the normal modes of CD_4 are smaller than for CH_4, which leads to higher thermal populations in excited vibrational states. If these excited states react more rapidly than the ground state, CD_4 would be expected to demonstrate a higher probability of reaction, an effect that would be counter to the observed isotope effect.

An alternative explanation for the observed KIE is related to quantum mechanical tunneling because hydrogen is lighter and has a higher probability of tunneling through a barrier than deuterium. An additional small effect (~7%) results from the difference in reduced mass between CD_4 and CH_4 because the

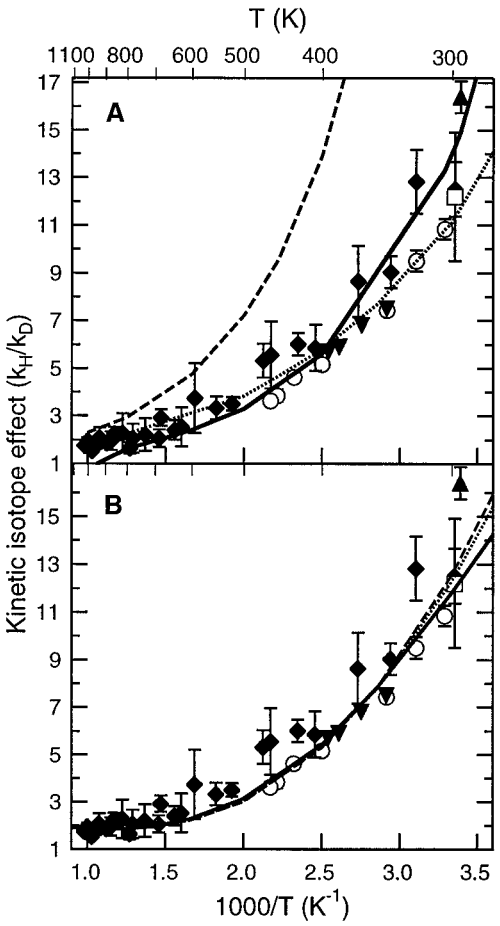

Figure 3. H/D kinetic isotope effect for Cl + CH_4/CD_4. Measured and calculated values of the KIE are shown as a function of inverse temperature. The KIE is expressed as a ratio of the rate constant for Cl + CH_4 (k_H) relative to the rate constant for Cl + CD_4 (k_D). The symbols represent measured values from (○) Chiltz et al.,[27] (♦) Clyne and Walker,[7] (▼) Vijn et al.,[50] (▲) Wallington and Hurley,[75] and (□) Matsumi et al.[25] (A) Lines represent calculated values from Espinosa-García and Corchado[33] (dashed), Roberto-Neto et al.[34] (dotted), and Corchado et al.[38] (solid). (B) Lines represent fits to data for case 1 (solid) and case 4 (dotted) assuming rates are enhanced by bending and stretching modes and for case 2 (dashed) assuming enhancement only by stretching modes.

collision frequency depends on the inverse square root of the reduced mass.

Simpson et al.[46] have shown that DCl produced by the reaction of Cl with $CD_4(v = 0)$ is more strongly backward scattered than (and as rotationally cold as) HCl produced via Cl reacting with $CH_4(v = 0)$. These results are consistent with those of Kandel and Zare,[44] which show that the CD_3 produced by Cl + $CD_4(v = 0)$ is more strongly forward scattered than (and as rotationally cold as) the CH_3 produced from Cl + CH_4-($v = 0$). These observations indicate that the ground-state reaction involving CD_4 may be more sterically constrained to a collinear geometry in the transition state than the reaction involving CH_4. A more sterically constrained transition state for Cl + CD_4 could also account for a lower probability of reaction for the deuterated isotope, which is qualitatively consistent with the observed H/D KIE.

Few theoretical studies have focused on the H/D KIE for Cl + CH_4.[27,33,34,38,74] Espinosa-García and Corchado,[33] Roberto-Neto et al.,[34] and Corchado et al.[38] used variational transition state theory to study the KIE for Cl + CH_4/CD_4. The results of these calculations are compared with the experimental values in Figure 3a. Despite the relatively good agreement between the measured rate constants and those calculated by Espinosa-García and Corchado[33] (Figure 1b), the corresponding calculated values for the KIE are significantly larger than the measured values. On the other hand, the calculations of Roberto-Neto et al.,[34] which demonstrate much poorer agreement with the measured absolute rate constants, yield good agreement with the measured KIE as do those of Corchado et al.[38] The calculations of Espinosa-García and Corchado[33] suggest that the high KIE at low temperatures is attributable to a combination of vibrational and tunneling effects, whereas the results of Roberto-Neto et al.[34] and Corchado et al.[38] indicate that tunneling contributes to the KIE but less so than predicted by Espinosa-García and Corchado.[33]

Analysis Methodology

Relating Differential Cross Sections to Rate Constants. In principle, differential cross sections can be used to derive thermal rate constants for a reaction with an activation barrier. To do so, measured state-dependent reaction cross sections must yield the reaction probability as a function of rotational, vibrational, electronic, and translational energy for all collision energies, orientations, and impact parameters. For the simple case in which all rotational, vibrational, and accessible electronic states react with equal probability and for which the translational energy dependence can be approximated by the line-of-centers model, the reactive cross section σ_R can be expressed in terms of a reaction probability P_{Rxn}, which is a function of an effective barrier height or threshold energy for reaction V and the net translational energy E_{trans},[1,45,73,80] i.e.,

$$\sigma_R = \sigma_{HS} P_{Rxn}(E_{trans},V) = A\sigma_{HS}\left(1 - \frac{V}{E_{trans}}\right) \qquad (1)$$

The normalization constant A is related to factors, such as steric restrictions, that limit the reactivity when E_{trans} exceeds V, and σ_{HS} is the hard-sphere collision cross section,

$$\sigma_{HS} = \pi d^2 \qquad (2)$$

where d is the hard-sphere minimum approach distance. An assumption of the line-of-centers model is that the reaction probability is constant for collision energies that exceed V. Figure 4 shows a comparison of P_{Rxn} given by the line-of-centers model for $V = 660$ cm^{-1} to a step function that switches at 660 cm^{-1}. Accounting for collisions with nonzero impact parameter causes P_{Rxn}, and thus eq 1, to deviate from a step function, as shown in Figure 4. A temperature-dependent rate constant $k(T)$ can be derived by multiplying σ_R by the normalized Maxwell distribution of speeds P_{Max} expressed in terms of E_{trans},

$$P_{Max}(T,E_{trans}) = \left(\frac{1}{k_B T}\right)^2 \left(\frac{8k_B T}{\pi\mu}\right)^{1/2} E_{trans} \exp\left(\frac{-E_{trans}}{k_B T}\right) dE_{trans} \qquad (3)$$

and integrating over all collision energies, i.e.,

$$k(T) = A\frac{Z}{(k_B T)^2}\int_0^\infty \left(1 - \frac{V}{E_{trans}}\right) E_{trans} \exp\left(\frac{-E_{trans}}{k_B T}\right) dE_{trans} \qquad (4)$$

In the expressions above, k_B is the Boltzmann constant, μ is the reduced mass, and Z is the collision frequency given by

$$Z(T) = \sigma_{HS}\left(\frac{8k_B T}{\pi\mu}\right)^{1/2} \qquad (5)$$

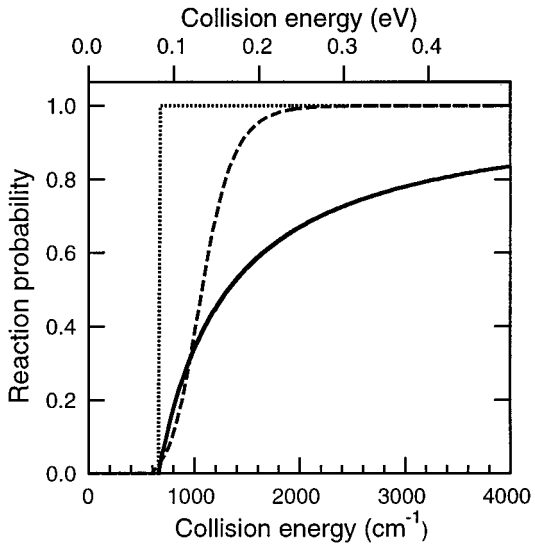

Figure 4. Energy dependence of the reaction probability. The reaction probability is shown as a function of collision energy for a step function that switches at 660 cm^{-1} (dotted line), for the line-of-centers model with $V = 660$ cm^{-1} (solid line), and for tunneling through a one-dimensional unsymmetrical Eckart potential barrier of 1150 cm^{-1} (dashed line).

Performing the integration in (4) gives the Arrhenius expression

$$k(T) = AZ \exp\left(\frac{-V}{k_B T}\right) \tag{6}$$

with a preexponential factor equal to AZ and an activation energy equal to V.

If the reaction cross section depends on the internal state of the reactants, as apparently is the case for Cl + CH_4, these equations must be solved for each state i using state-dependent values for the normalization A_i and effective barrier V_i. The total rate constant is calculated by summing over all states. The result is a multiexponential expression given by

$$k(T) = \sum_i S_i A_i Z \exp\left(\frac{-V_i}{k_B T}\right) \tag{7}$$

where S_i represents the population in state i. Populations are given by a Boltzmann distribution, i.e.,

$$S_i = \frac{G_i \exp\left(\frac{-\Delta E_i}{k_B T}\right)}{\sum_j G_j \exp\left(\frac{-\Delta E_j}{k_B T}\right)} \tag{8}$$

where ΔE_i is the difference in energy between the ground state and internal state i, and G_i is the degeneracy of state i (the degeneracy of the vibrational mode g corrected for the number of vibrational quanta).

For the Cl + CH_4 reaction, insufficient dynamical information is available to derive rate constants directly from measured relative state-dependent reaction cross sections. Nevertheless, the available dynamical information can be used to develop a realistic expression to fit to the measured rate constants by making several physically reasonable simplifying assumptions. For the first part of the analysis presented here, we used eq 1 to describe the translational energy dependence of the reaction probability for individual vibrational states of CH_4 and assumed that the reaction probability is independent of CH_4 rotational state.

TABLE 1: Frequencies and Degeneracies of Normal Modes of CH_4[81] and CD_4[82]

			frequency (cm^{-1})	
	mode	g	CH_4	CD_4
symmetric stretch	υ_1	1	2916.47	2084.7
torsional bend	υ_2	2	1533.33	1091.6
asymmetric stretch	υ_3	3	3019.50	2258.2
umbrella bend	υ_4	3	1310.76	995.6

Methane has four normal vibrational modes (summarized in Table 1). The stretching modes are nearly iso-energetic, as are the bending modes.[81,82] Because the symmetric and asymmetric stretching modes provide similar motion along the reaction coordinate, we assumed that the reaction probability is the same for υ_1 and υ_3, although the population was calculated separately for each state. The umbrella bending mode is also expected to couple to the reaction coordinate,[31] and we assumed a separate reaction probability for υ_4. Because the torsional bending mode is not expected to couple strongly to the reaction coordinate,[31] we assumed that this mode did not enhance the reactivity. We also assumed that the higher overtones have the same reaction probability as (but significantly lower population than) the fundamental for each mode. With these assumptions, eq 7 has three terms corresponding to vibrational modes of CH_4: one for the ground state and excited υ_2 mode, one for the excited υ_4 mode, and one for the excited υ_1 and υ_3 modes.

We performed Levenberg−Marquardt nonlinear least-squares fits of this equation to the data, weighted by the inverse of the estimated total (1σ) uncertainty of the measurements. We excluded from these fits data sets with room-temperature rate constants that are more than two standard deviations ($2\sigma = 2.36 \times 10^{-14}$ cm^3 $molecule^{-1}$ s^{-1}) from the weighted mean (1.030×10^{-13} cm^3 $molecule^{-1}$ s^{-1}).[2,7,8,19] Each fit was performed using five adjustable parameters: the normalization factors for each term, $A_{0,2}$, A_4, and $A_{1,3}$, and the threshold values for reaction of the ground state and excited υ_2 mode $V_{0,2}$ and the excited υ_4 mode V_4. Because the stretching motion is well coupled to the reaction coordinate, and a vibrational quantum for the stretch far exceeds the estimated reaction barrier height, we assumed the threshold for the stretching modes was zero (except for the fits assuming no vibrational enhancement of the rate constant). All fits for which V_4 was allowed to vary independently yielded a value of zero for V_4. For the fits presented in the following section, we constrained V_4 to zero for ease of convergence when the bend was assumed to enhance the reaction rate. We turned the bending mode off (neglected possible enhancement from this mode) by constrainig V_4 to be equal to $V_{0,2}$ and A_4 to be equal to $A_{0,2}$. We similarly turned the stretching modes off by constraining $V_{1,3}$ to be equal to $V_{0,2}$ and $A_{1,3}$ to be equal to $A_{0,2}$.

This model does not account for attractive intermolecular forces. For this system, however, these forces are expected to be negligible.[83] Equation 7 also neglects contributions to the rate constants from tunneling, which may be significant at low temperatures for hydrogen abstraction reactions. We performed additional fits to the data using eq 4 modified by a tunneling transmission coefficient $\kappa(E_{trans},V_i)$ to represent the probability of reaction for each state. Equation 7 thus becomes

$$k(T) = \sum_i \frac{S_i A_i Z}{(k_B T)^2} \int_0^\infty \kappa(E_{trans},V_i) E_{trans} \exp\left(\frac{-E_{trans}}{k_B T}\right) dE_{trans} \tag{9}$$

The functional form used for the transmission coefficient (and shown in Figure 4 for a barrier of 1150 cm^{-1}) is based on a one-dimensional unsymmetrical Eckart potential energy function as described by Eckart[84] and Johnston and Heicklen.[85] To estimate the curvature at the maximum of this function, we used the imaginary stretching frequency of the transition state along the reaction coordinate given by the mean of values from several theoretical studies (1000i cm^{-1}).[28,30−35,86] This approach is tractable but does not account for motion orthogonal to the reaction coordinate,[85] which may lead to errors because multidimensional tunneling is expected to be significant.[31,33,34] In our analysis, uncertainties in the tunneling coefficients should only affect the ground-state/torsional mode parameters, and errors associated with neglecting multidimensional tunneling should be, at least partially, compensated by adjustments in $A_{0,2}$ and $V_{0,2}$.

To compare the results of the fits with the state-dependent enhancement factors F_{Exp} measured for the stretch[46] and bend,[44] we integrated P_{Rxn} for each state over the estimated experimental collision energy spread and calculated the ratio for the excited state relative to the ground state, i.e.,

$$F_{Exp} = \frac{A_i \int_0^\infty \kappa(E_{trans},V_i) P_{Exp}\, dE_{trans}}{A_{0,2} \int_0^\infty \kappa(E_{trans},V_{0,2}) P_{Exp}\, dE_{trans}} \qquad (10)$$

where P_{Exp} is the distribution of collision energies, which depends on the reduced mass of the reactants and the photolysis wavelength used to generate chlorine atoms.[87] For comparison of our model results with calculated enhancement factors, the temperature-dependent enhancement factors $F_{Calc}(T)$ were referenced to the thermal rate constants, i.e.,

$$F_{Calc}(T) = \frac{A_i \int_0^\infty \kappa(E_{trans},V_i) E_{trans} \exp\left(\frac{-E_{trans}}{k_B T}\right) dE_{trans}}{\sum_i S_i A_i \int_0^\infty \kappa(E_{trans},V_i) E_{trans} \exp\left(\frac{-E_{trans}}{k_B T}\right) dE_{trans}} \qquad (11)$$

Kinetic Isotope Effect. We included measurements of the KIE for $Cl + CH_4/CD_4$ in our analysis by performing separate fits to these data to extract values of $A_{0,2}$, A_4, $A_{1,3}$, $V_{0,2}$, and V_4 for CD_4. We used the equations described above with isotope-specific values for these parameters to represent the rate constants for each reaction. For $Cl + CH_4$, these parameters were constrained to the values derived from the fits to the thermal rate constant data, and for $Cl + CD_4$, these parameters were allowed to vary. The endothermicity of this reaction was assumed to be 900 cm^{-1} based on the ZPE of the reactants[81,82] relative to the products.[88−92] The normal mode vibrational frequencies for CD_4 are given in Table 1. The value of V_4 was not allowed to be less than a vibrational quantum of the bending mode (996 cm^{-1}) lower than $V_{0,2}$. For the tunneling approximation, we assumed an imaginary frequency of the transition state along the reaction coordinate of 750i cm^{-1}, based on calculations by Roberto-Neto et al.[34] We assumed that the hard sphere collision cross section for the reaction involving CD_4 was the same as that for CH_4 but corrected the collision frequency to account for the difference in the reduced mass of the reacting pair.

Results

Fits to Thermal Rate Constants. We performed fits to the thermal rate constant measurements for the six cases summarized in Table 2. For cases 1 and 4, we assumed that the symmetric and asymmetric stretch and umbrella bend modes enhanced the reaction rate. For cases 2 and 5, we assumed that only the stretching modes enhanced the reaction rate, and for cases 3 and 6, we assumed that vibrational motion did not enhance the reaction rates. Tunneling was taken into account for cases 4, 5, and 6 but not for cases 1, 2, and 3. The results are shown in Figure 5.

TABLE 2: Parameters Given by Fit to Thermal Rate Constant Data for $Cl + CH_4$

	case 1	case 2	case 3	case 4	case 5	case 6
stretch	on	on	off	on	on	off
bend	on	off	off	on	off	off
tunneling	off	off	off	on	on	on
$V_{0,2}$ (cm^{-1})	660	795	890	1150	1230	1350
V_4 (cm^{-1})	0	795	890	0	1230	1350
$V_{1,3}$ (cm^{-1})	0	0	890	0	0	1350
$A_{0,2}$	0.007	0.017	0.027	0.007	0.010	0.017
A_4	0.011	0.017	0.027	0.007	0.010	0.017
$A_{1,3}$	0.150	0.167	0.027	0.186	0.175	0.017
χ^2	1.64	1.40	3.81	1.43	1.40	4.04

For high temperatures (>300 K), the curvature observed in the Arrhenius plot is reproduced equally well by cases 1 and 2 and is not reproduced by case 3 (Figure 5a). Figure 6a shows the contributions to the calculated rate constants from the different vibrational modes for case 1, and Figure 6b shows the individual vibrational components for case 2. Within the constraints of this model, vibrational enhancement of the reaction rate is needed to explain the non-Arrhenius behavior at high temperatures. At temperatures above ~600 K, enhancement by the stretching modes alone can explain the non-Arrhenius behavior, and enhancement by the low-frequency bending modes is not required. The cases for which the tunneling was taken into account (Figures 5c and 6c) demonstrate agreement similar to that shown by the corresponding cases that neglected tunneling effects.

At low temperatures, fits to the data are again poor if vibrational enhancement of the reaction rate was neglected, whether tunneling was included or neglected. As shown in Figures 5b and 5d, cases 3 and 6 yielded results that are lower than a majority of the measured rate constants at temperatures below 250 K. The most important factor determining the quality of the fit (as indicated by the values of χ^2 given in Table 2)[93] was whether the model had a way to account for curvature in the data, particularly at high temperature where the curvature is more pronounced. Although cases 3 and 6 account for the temperature dependence of the preexponential factor associated with the temperature dependence of the collision frequency, this variability with temperature is not sufficient to account for the non-Arrhenius behavior observed. Thus, the worst fits were obtained when contributions from the stretching modes, which control the curvature at high temperatures, were neglected, and the best fits were obtained when contributions from the stretching modes and either the bending modes or tunneling, both of which can provide curvature at low temperatures, were included. When tunneling was included, the fit neglecting enhancement by the bend was only marginally better than that including the bend.

Kinetic Isotope Effect. The results of fits to the KIE data for $Cl + CH_4/CD_4$ are shown in Figure 3b and summarized in Table 3. Because cases 3 and 6 did not provide acceptable fits to the rate constants for $Cl + CH_4$, we excluded these cases from the KIE analysis. Fits for the other four cases yielded comparably good agreement with the measurements. Results for case 5 falls on top of the case 2 curve and was excluded

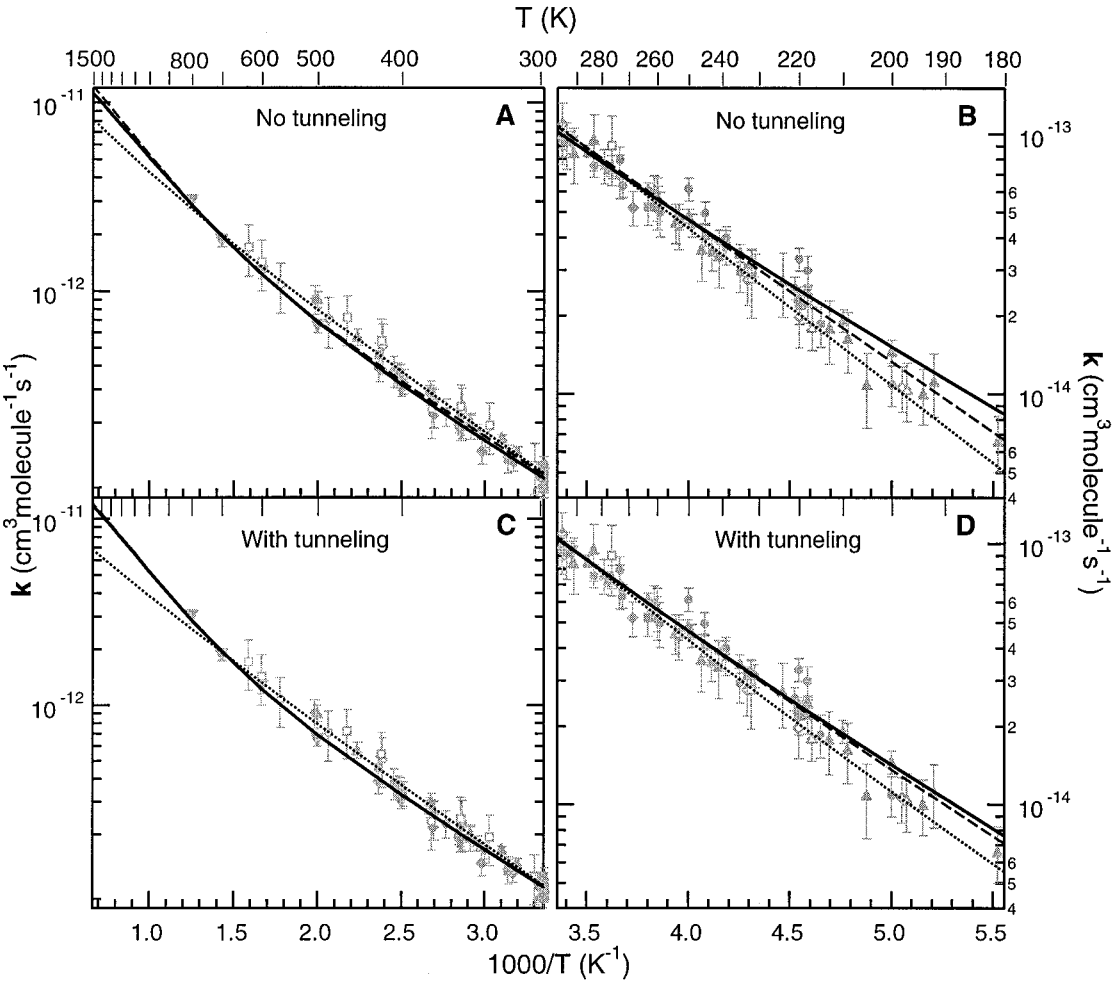

Figure 5. Comparison of measured rate constants with fits assuming vibrational state-dependent reaction cross sections. The data (gray symbols) used in the fit are the same as shown in Figure 1 excluding measurements from Lee and Rowland,[2] Clyne and Walker,[7] Poulet et al.,[8] and Davis et al.[19] Lines represent results of fits to the data for the cases summarized in Table 2: (A) and (B) case 1 (solid) assuming both stretching modes and the umbrella bending mode enhance reactivity, case 2 (dashed) assuming only the stretching modes accelerate the reaction, case 3 (dotted) assuming that the reaction is not vibrationally enhanced; (C) and (D) case 4 (solid) assuming both stretching modes and the umbrella bending mode enhance reactivity, case 5 (dashed) assuming only the stretching modes accelerate the reaction, case 6 (dotted) assuming that the reaction is not vibrationally enhanced.

from Figure 3b for clarity. For the KIE data shown here, including enhancement by the bend gave slightly better agreement with the data.

Discussion

The results of the fits to the thermal rate constants for Cl + CH_4 demonstrate several general trends. Values of V_i for the cases including tunneling are 435−490 cm^{-1} higher than threshold energies for the corresponding cases that do not account for tunneling. Figure 4 shows a comparison of the normalized ground-state reaction probability for case 1 ($V_{0,2}$ = 660 cm^{-1}) with the ground-state transmission function for case 4 ($V_{0,2}$ = 1150 cm^{-1}). Although the value of $V_{0,2}$ is 490 cm^{-1} higher for case 4, tunneling allows the reaction to occur at energies much lower than $V_{0,2}$, such that the functions are similar in magnitude at collision energies below 1000 cm^{-1}. This example shows that for an activated reaction for which the reaction probability is independent of internal state and unaffected by tunneling, the barrier height (relative to the zero-point energy) and the activation energy (corrected for the collision rate) should be comparable. If tunneling is important, the activation energy can be significantly lower than the barrier height.[1] Differential reactivity of reactant internal states and other consequences of the multidimensional aspects of the PES may also lead to decreases in the activation energy relative to the barrier height.[34] For reactions strongly influenced by such factors, the activation energy is not a good first-order approximation for the barrier height.

Our value of $V_{0,2}$ for case 3 is in good agreement with previously derived activation energies.[56,57] This agreement is expected because these earlier values were derived by a fit using a single-exponential function. Values of $V_{0,2}$ for cases 1 and 2 are lower than reported activation energies, and values for cases 4, 5, and 6 are significantly higher. These latter values of $V_{0,2}$ are more consistent with theoretical estimates of the barrier height, which fall in the range of 1220−1700 cm^{-1},[28,30,31,33,35−38] providing evidence that tunneling is important for this reaction.

The influence of tunneling increases with decreasing temperature, as demonstrated by the temperature dependence of the tunneling corrections. Figure 7a shows tunneling enhancement factors, calculated based on eq 18 from Johnston and Heicklen,[85] compared with tunneling factors produced by more detailed theoretical studies. Considering that we have not accounted for curvature along the reaction coordinate, the agreement between our results and other theoretical values is remarkably good. The most significant (unexplained) discrepancy is between the results

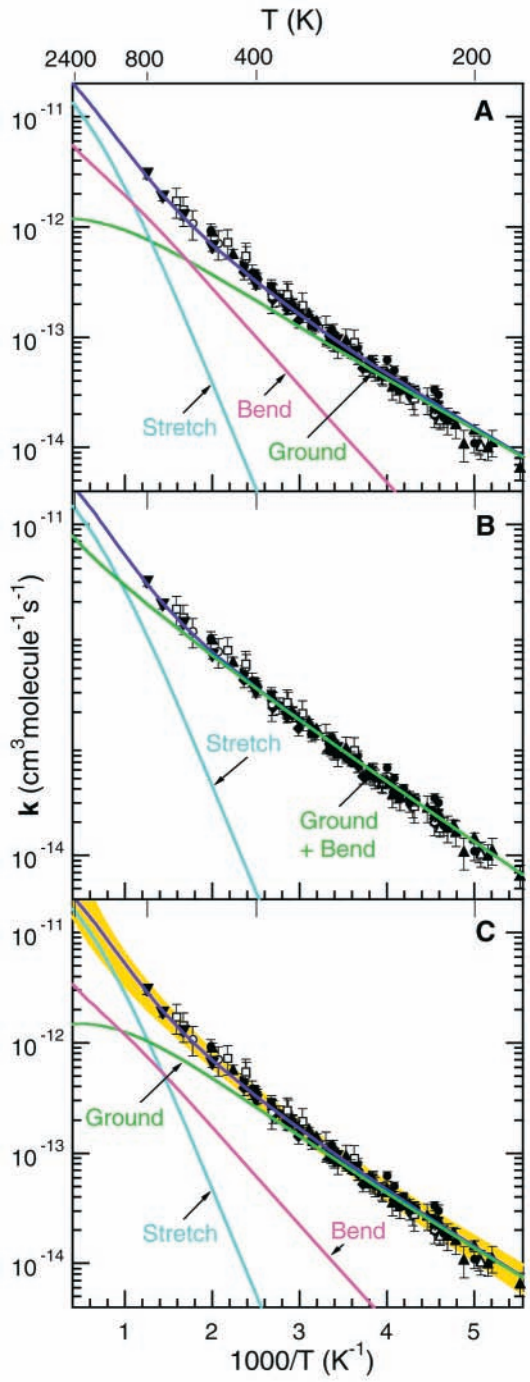

Figure 6. Comparison of measured rate constants with fits assuming vibrational state-dependent reaction cross sections. The data (black symbols) used in the fit are the same as shown in Figure 1 excluding measurements from Lee and Rowland,[2] Clyne and Walker,[7] Poulet et al.,[8] and Davis et al.[19] Solid lines represent results of fits to the data shown: the contribution to the rate constants from the ground-state reaction and excited torsional mode (green), from excitation of the CH_4 stretching modes (cyan), from excitation of the umbrella bending mode (magenta), and from the sum of all states (purple). The fits were from the following cases presented in Table 2: (A) assuming contributions from both stretching and umbrella bending modes with no tunneling (case 1), (B) assuming contributions from just the stretching modes with no tunneling (case 2), and (C) assuming contributions from both stretching and umbrella bending modes with tunneling (case 4).

of Espinosa-García and Corchado[33] and the other theoretical values. The high values for the H/D KIE calculated by Espinosa-García and Corchado[33] (Figure 3a) may be attributable to these large tunneling factors.

TABLE 3: Parameters Given for Cl + CD_4 by Fit to KIE Data

	case 1	case 2	case 4	case 5
$V_{0,2}$ (cm^{-1})	980	1230	1420	1650
V_4 (cm^{-1})	0	1230	425	1650
$V_{1,3}$ (cm^{-1})	0	0	0	0
$A_{0,2}$	0.00067	0.0091	0.00030	0.00485
A_4	0.00070	0.0091	0.00157	0.00485
$A_{1,3}$	0.0875	0.072	0.084	0.070
χ^2	3.4	3.5	3.4	3.5

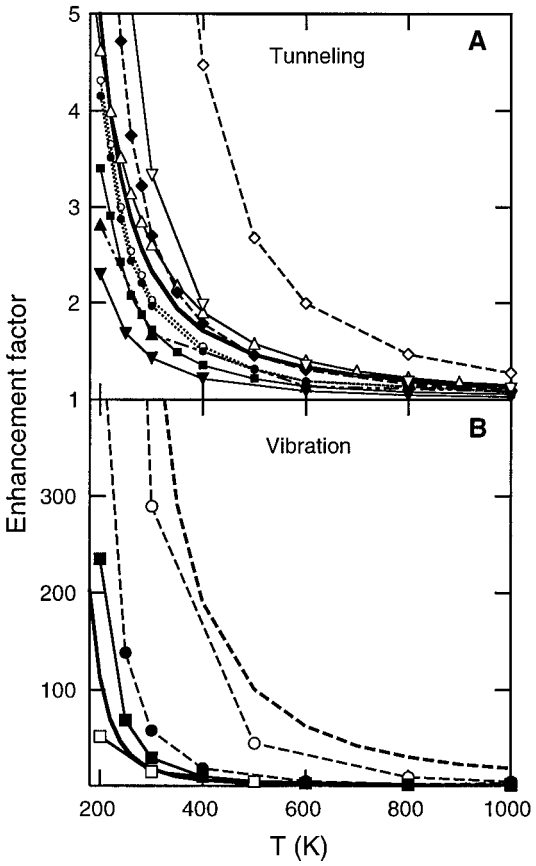

Figure 7. Comparison of theoretical and empirical enhancement factors. (A) Tunneling correction factors are shown for our results (plain solid line) and for calculations by Yu and Nyman[36] based on Wigner transmission coefficients (solid line with triangles), Gonzalez-Lafont et al.[29] assuming small curvature tunneling (dot−dashed line with solid triangles), Duncan and Truong[31] assuming small curvature tunneling (solid line with squares), Roberto-Neto et al.[34] assuming small curvature tunneling (dotted line with closed circles) and large curvature tunneling (dotted line with open circles), Espinosa-García and Corchado[33] assuming small curvature tunneling (dashed line with closed diamonds) and large curvature tunneling (dashed line with open diamonds), and Corchado et al.[38] assuming small curvature tunneling (solid line with closed inverted triangles) and large curvature tunneling (solid line with open inverted triangles). (B) The temperature dependence of the reaction rate enhancement by stretching (dashed) and bending (solid) modes is shown for our results based on case 4 (thick lines) and for calculations by Duncan and Truong[31] (thin lines with open symbols) and Corchado et al.[38] (thin lines with closed symbols).

Further evidence for the importance of tunneling is provided by the parameters derived from the KIE measurements. For all cases, $V_{0,2}$ is higher for Cl + CD_4 than for Cl + CH_4. For case 4 this difference is within the uncertainty of the expected values of $\Delta V_{0,2}$ (+310 to −380 cm^{-1}) based on the differences in the zero-point energies of the reactants and transition state (estimated from theoretical values given by Roberto-Neto et al.[34]); the differences are larger for the other cases. For each case, $A_{1,3}$ (the normalization or steric factor for the stretching modes)

is a factor of ~2 smaller for the reaction with CD_4. Values of $A_{0,2}$ and A_4 are also smaller (by factors of 2−23) for reaction with the heavier isotope. These results, combined with the results of the differential cross-section measurements for the different isotopes, indicate that tunneling effectively opens the cone of acceptance for this reaction. The geometry of the transition state appears to be less tightly constrained for CH_4 than for CD_4, allowing $A_{1,3}$, $A_{0,2}$, and A_4 to be larger and the reaction probability to be higher. Because our model only accounts explicitly for tunneling along the reaction coordinate, such a mechanism involving components orthogonal to this coordinate is instead reflected in the normalization factor. These results are consistent with a more extensive analysis of the H/D and carbon KIE data for this reaction.[94]

The evidence presented above indicates that (1) vibrational enhancement of the reaction probability by the stretching modes of CH_4 strongly influences the reaction rate at high temperatures, and (2) tunneling contributes to the reaction rate at low temperatures. Overall case 4 yields a better fit to the thermal rate constant and KIE data than the other cases, but the agreement is only marginally better than for case 5 for which the contribution to the rate constant from the bending mode is neglected. Given that several studies have suggested that low-frequency bending modes enhance the reactivity,[44,47−49] we assume case 4, which includes such contributions, provides the most realistic representation of this system.

For case 4, the normalization for the stretch is ~27 times larger than the normalization for the ground-state reactants. Using eq 10, we find that excitation of the stretch enhances the reaction probability by a factor of 36 at a collision energy of 1274 cm^{-1}, which is in good agreement with the value of 30 ± 15 (2σ) given by Simpson et al.[46]

The normalization for the bend, on the other hand, is much smaller than that of the stretch and is comparable to the normalization for the ground state. These results are inconsistent with the conclusion of Kandel and Zare[44] that excitation of the bend is more effective at promoting this reaction than excitation of the stretch. We find that the bend enhances the reaction probability by factors of ≤2 at collision energies between 1040 and 1961 cm^{-1}, approximately 2 orders of magnitude smaller than the enhancement factors estimated by Kandel and Zare.[44] In these calculations we have assumed that the torsional bending modes do not enhance the reaction rate. Including enhancement by the torsional mode effectively increases the population of the active low-frequency bending states, which leads to a net reduction in the normalization factor and a lower enhancement factor for the bend. Thus, if the torsion enhances the reaction rate, our estimate of the enhancement factor for the bend (neglecting the contribution from the torsional mode) is too high, and the discrepancy between our results and those of Kandel and Zare[44] is even more significant. Furthermore, based on the assumption that Simpson et al.[46] had neglected to account for vibrational enhancement by the bend in deriving this value, Kandel and Zare[44] calculated that the enhancement by the stretch was closer to 120; this value is 3 times larger than can be accommodated by our analysis of the rate constants. Although we have no alternative explanation for the high translational energy of the products observed by Kandel and Zare,[44] we are unable to reconcile the interpretation thus far provided for these data with the thermal rate constant measurements. Nevertheless, these inconsistencies do not rule out the possibility that the bend makes a distinct contribution to the reaction probability.

Our results are qualitatively consistent with the rate enhancement by bend and stretch excitation (relative to thermal rate constants) calculated by Duncan and Truong,[31] but quantitatively our enhancement factors are generally higher (Figure 7b). The enhancement factors for the bend are in good quantitative agreement at room temperature and above, but the bend enhancement calculated by Duncan and Truong[31] at 200 K is a factor of 2.2 lower than our value. Our enhancement factors for the stretch are 1.7−3.5 times higher. Agreement is not as good with calculations by Corchado et al.[38] for which enhancement by the stretch is much lower and enhancement by the bend is much higher than our results and those of Duncan and Truong.[31]

A note of caution should be applied to analyses of low-temperature rate constant measurements for this reaction. Methane has long been known to undergo electronic excitation into the 3*s* Rydberg state by absorption of light at wavelengths in the range of those produced by the lamp used for Cl resonance fluorescence detection.[95−97] Recent studies have shown that, following excitation to the 3*s* Rydberg state, CH_4 is much more likely to dissociate than to relax to a lower electronic state, yielding CH_3, CH_2, H, and H_2.[96−101] Thus, if the reaction rate of Cl with any of these fragments (or with byproducts of secondary reactions of these fragments) is faster than the reaction with CH_4, the inferred rate will be higher than the actual rate of Cl + CH_4 in experiments where the reaction is monitored by the loss of Cl. All data currently available for temperatures below 233 K were obtained using resonance fluorescence detection of Cl. Only one study using an alternative technique has been published for temperatures below 268 K.[11] A detailed investigation of the implications will require additional experimental studies, including studies using alternative detection techniques.

To facilitate the use of these results in atmospheric and combustion models, we have extrapolated the results of our fit to the data with a prediction based on case 4 (our best representation of the data) and fit the results between 180 and 2500 K using a simple functional form. This curve is fit to within ±4% (within ±1.5% at $T \leq$ 350 K) by the expression

$$k(T) = 2.50 \times 10^{-11}\left(\frac{298}{T}\right)^{1.006} \exp\left[\frac{-1827.9}{T} + \left(\frac{222.1}{T}\right)^2\right] + 1.21 \times 10^{-11}\left(\frac{298}{T}\right)^{0.216} \exp\left(\frac{-2080.3}{T}\right) + 3.53 \times 10^{-9}\left(\frac{298}{T}\right)^{1.544} \exp\left[\frac{-5349.6}{T} + \left(\frac{259.59}{T}\right)^2\right] \quad (12)$$

For a temperature T in Kelvin, the rate constant is given in cm^3 $molecule^{-1}$ s^{-1}. The first term represents the contribution from the CH_4 vibrational ground state, the second term represents the contribution from the umbrella bending mode, and the third term represents the contribution from the stretching modes. The residuals of this fit are shown in Figure 8a as percent differences. For comparison with other studies, we have also performed a fit using a common expression for describing the temperature dependence of the rate constants, i.e.,

$$k(T) = 2.506^{-1.275}_{+0.711} \times 10^{-12}\left(\frac{T}{298}\right)^{1.27^{+0.68}_{-0.38}} \times \exp\left[\frac{-(938.31^{-244.57}_{+134.79})}{T}\right] \quad (13)$$

Although eq 12 provides a better fit to the case 4 curve, eq 13 reproduces this curve to within ±15% below 2400 K and within ±3% between 200 and 300 K. Because of the large scatter in the measurements at low temperature and the lack of measure-

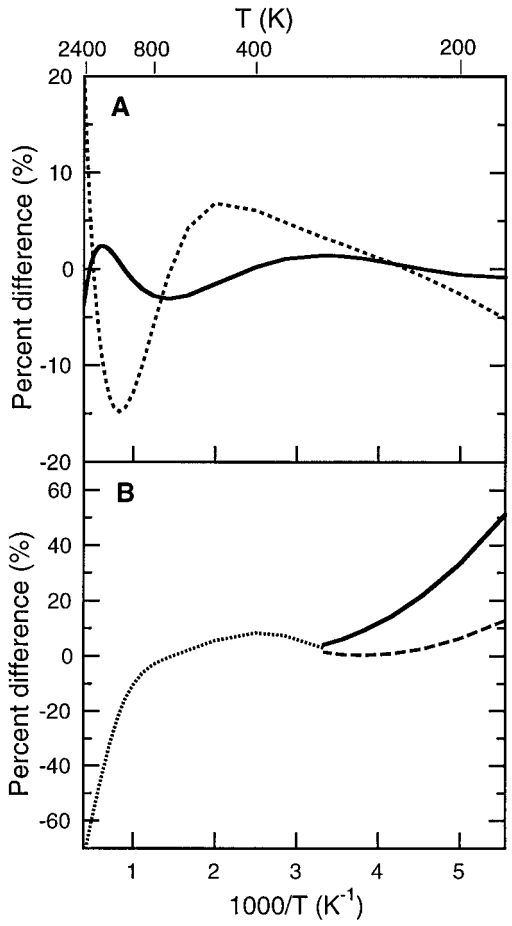

Figure 8. Comparison of recommended rate constants. (A) Percent differences are defined as $(100\%)(k_{eqn} - k_{case4})/k_{case4}$ and shown as a function of temperature for eq 12 (solid line) and eq 13 (dotted line). (B) Percent differences, defined as $(100\%)(k_{case4} - k_{rec})/k_{rec}$, are shown for recommended values from Sander et al.[56] (solid line), Atkinson et al.[57] (dashed line), and Pilgrim et al.[24] (dotted line).

ments at high temperatures, uncertainties are difficult to assess. The error bars given in eq 13 and shown in Figure 6c conservatively encompass data within 2σ of the mean measured value at each temperature.

The differences between our results and values recommended by Sander et al.[56] are significant, as much as 51% at 180 K, as shown in Figure 8b. The differences are much smaller (within 13%) between our results and values recommended by Atkinson et al.[57] At temperatures between 300 and 800 K, our results agree to within 5% with the expression given by Pilgrim et al.[24] but diverge sharply above 800 K, suggesting that the rate constant cannot be readily extrapolated from a simple Arrhenius-type fit to the measurements.

Atmospheric Implications

Under most conditions in the lower stratosphere, the majority of inorganic chlorine is partitioned predominantly into the relatively stable species HCl and $ClNO_3$ (60−80% HCl and 20−40% $ClNO_3$ at 20 km).[42,102−104] Abundances of ClO and HCl increase with altitude at the expense of $ClNO_3$, such that in the upper stratosphere inorganic chlorine is predominantly ClO and HCl (∼80% HCl and ∼15% ClO at 40 km).[42,104−106] An increase in the estimated rates for the Cl + CH_4 reaction at low temperatures has previously been shown to have a substantial impact on the partitioning of inorganic chlorine predicted for the middle and upper stratosphere.[42] For example, an increase in the rate constants of this reaction, similar in magnitude to the increase over the current NASA recommendations[56] suggested by our results, was shown to decrease the predicted relative abundances of $ClNO_3$ and HCl by 15−20% in the middle stratosphere.

The increase in the estimated rates of Cl + CH_4 at low temperature is also expected to have an effect on the predicted recovery rate of the chemically perturbed springtime lower stratospheric polar vortex. During the polar winter when temperatures drop below ∼195 K, HCl and $ClNO_3$ are heterogeneously converted to Cl_2, which is then photolyzed to produce reactive chlorine radicals if sunlight is available (or when it becomes available).[107−111] These radicals participate in the catalytic destruction of polar ozone during the late winter and early spring.[112−114] As temperatures increase in the spring, these heterogeneous reactions cease, and chlorine radicals are reconverted to HCl and $ClNO_3$. If ozone has been severely depleted in the vortex (e.g., in the Antarctic vortex), HCl is preferentially produced, and the rate of conversion of reactive radicals to HCl is predominantly controlled by the rate of Cl + CH_4.[103,115−119] If ozone has not been completely depleted (e.g., in the Arctic vortex), the partitioning between HCl and $ClNO_3$ in the initial stage of recovery will depend on the relative rates of Cl + CH_4 and ClO + NO_2, the latter of which produces $ClNO_3$.[111,115,116,119] $ClNO_3$ is less photochemically stable than HCl, and photolysis of $ClNO_3$ regenerates chlorine radicals. An increase in the rate of Cl + CH_4 used in models will thus lead to an increase in the calculated rate of recovery of the chlorine partitioning to the steady-state conditions (HCl > $ClNO_3$) and to a decrease in the projected cumulative loss of ozone during the polar spring.

Conclusions

We have fit available measured rate constants for the Cl + CH_4 reaction using a model that accounts for enhancement of the reaction rate by excited vibrational states of CH_4. Our results are in good agreement with the work of Simpson et al.,[45,46] which demonstrated that the reaction rate is enhanced by energy in the asymmetric stretch mode (by a factor of 30 at a collision energy of 1274 cm^{-1}). Vibrational enhancement by the stretching modes appears to be responsible for the non-Arrhenius behavior observed at temperatures between 300 and 800 K. Our results suggest that the curvature in the Arrhenius plot at low temperatures is attributable to both tunneling and a small amount of enhancement of the reaction rate by excitation of a low-frequency bending mode. The magnitude of the enhancement by the bend is much smaller than suggested by Kandel and Zare,[44] but the relative contributions to the reaction rate by stretching and bending modes are consistent with theoretical predictions by Duncan and Truong.[31] An analysis of the kinetic isotope effect for Cl + CH_4/CD_4 indicates that tunneling relaxes the tight steric constraints for collinearity in the transition state and effectively opens the cone of acceptance for the ground-state reaction. Our best estimate for the rate constant, based on this analysis of the measured rate constants, is higher than current recommendations by as much as 51% at 180 K. This analysis also yields a prediction for rate constants at temperatures higher than 800 K, the highest temperature for which measurements are currently available.

The model we have used to fit the rate constant data is based on state-dependent experimental results and is therefore more physically realistic than a standard Arrhenius expression. Nevertheless, understanding details of the mechanisms that control the rates for this reaction is critical to confirming the results presented here. There are several obvious theoretic and

experimental studies that would provide information necessary to understand these mechanisms. (1) The methodology employed in this study could be greatly improved with a more reliable estimate of the reaction probability function to be used in the fit to the data. This analysis could benefit from incorporating theoretical predictions of the multidimensional transmission function. (2) State-dependent reaction dynamics studies at lower collision energies are needed to explore the contributions of the bend and stretch modes to the reaction probability. (3) Thermal rate constant measurements made at temperatures higher than 800 K will aid in the identification of the role of the stretching modes in determining the reaction probability. (4) Measurements of the absolute rate constants at low temperatures should be made using techniques other than resonance fluorescence detection. There is currently only one published study that has used an alternative technique for temperatures below 268 K[11] and none below 233 K. (5) Studies should be performed of the implications of electronic excitation of CH_4 by absorption of the lamp emission (∼135 nm) used to detect Cl via resonance fluorescence. (6) The H/D kinetic isotope effect for Cl + CH_4/CD_4 should be investigated at lower temperatures where tunneling is expected to be more important.

Acknowledgment. We thank R. L. Farrow, D. M. Golden, S. A. Kandel, D. A. V. Kliner, A. McIlroy, D. L. Osborn, A. R. Ravishankara, C. A. Taatjes, D. W. Toohey, and F. P. Tully for enlightening discussions and helpful suggestions. This work was supported by the U. S. Department of Energy, Office of Basic Energy Sciences, Division of Chemical Sciences and the National Aeronautics and Space Administration, Atmospheric Chemistry Modeling and Analysis Program.

References and Notes

(1) (a) Johnston, H. S. *Gas-Phase Reaction Rate Theory*; The Ronald Press: New York, 1966; pp 38−47. (b) Steinfeld, J. I.; Francisco, J. S.; Hase, W. L. *Chemical Kinetics and Dynamics*, 2nd ed.; Prentice Hall: Upper Saddle River, NJ, 1999; pp 248−250, 318−321.

(2) Lee, F. S. C.; Rowland, F. S. *J. Phys. Chem.* **1977**, *81*, 86.

(3) (a) Pritchard, H. O.; Pyke, J. B.; Trotman-Dickenson, A. F. *J. Am. Chem. Soc.* **1954**, *76*, 1201. (b) Pritchard, H. O.; Pyke, J. B.; Trotman-Dickenson, A. F. *J. Am. Chem. Soc.* **1955**, *77*, 2629.

(4) (a) Knox, J. H. *Chem. Ind.* **1955**, 1631. (b) Knox, J. H.; Nelson, R. L. *Trans. Faraday Soc.* **1959**, *55*, 937.

(5) DeMore, W. B. *J. Geophys. Res.* **1991**, *96*, 4995.

(6) Lin, C. L.; Leu, M. T.; DeMore, W. B. *J. Phys. Chem.* **1978**, *82*, 1772.

(7) Clyne, M. A. A.; Walker, R. F. *J. Chem. Soc., Faraday Trans. 1* **1973**, *69*, 1547.

(8) Poulet, G.; Bras, G. L.; Combourieu, J. *J. Chim. Phys.* **1974**, *71*, 101.

(9) Sawersyn, J.-P.; Lafage, C.; Meriaux, B.; Tighezza, A. *J. Chim. Phys.* **1987**, *84*, 1187.

(10) Baghal-Vayjooee, M. H.; Colussi, A. J.; Benson, S. W. *J. Am. Chem. Soc.* **1978**, *100*, 3214.

(11) Heneghan, S. P.; Knoot, P. A.; Benson, S. W. *Int. J. Chem. Kinet.* **1981**, *13*, 677.

(12) Dobis, O.; Benson, S. W. *Int. J. Chem. Kinet.* **1987**, *19*, 691.

(13) Keyser, L. F. *J. Chem. Phys.* **1978**, *69*, 214.

(14) Zahniser, M. S.; Berquist, B. M.; Kaufman, F. *Int. J. Chem. Kinet.* **1978**, *X*, 15.

(15) Michael, J. V.; Lee, J. H. *Chem. Phys. Lett.* **1977**, *51*, 303.

(16) Beichert, P.; Wingen, L.; Lee, J.; Vogt, R.; Ezell, M. J.; Ragains, M.; Neavyn, R.; Finlayson-Pitts, B. J. *J. Phys. Chem.* **1995**, *99*, 13156.

(17) Seeley, J. V.; Jayne, J. T.; Molina, M. J. *J. Phys. Chem.* **1996**, *100*, 4019.

(18) Wang, J. J.; Keyser, L. F. *J. Phys. Chem. A* **1999**, *103*, 7460.

(19) Davis, D. D.; Braun, W.; Bass, A. M. *Int. J. Chem. Kinet.* **1970**, *II*, 101.

(20) Watson, R.; Machado, G.; Fischer, S.; Davis, D. D. *J. Chem. Phys.* **1976**, *65*, 2126.

(21) Manning, R. G.; Kurylo, M. J. *J. Phys. Chem.* **1977**, *81*, 291.

(22) Whytock, D. A.; Lee, J. H.; Michael, J. V.; Payne, W. A.; Stief, L. J. *J. Phys. Chem.* **1977**, *66*, 2690.

(23) Ravishankara, A. R.; Wine, P. H. *J. Chem. Phys.* **1980**, *72*, 25.

(24) Pilgrim, J. S.; McIlroy, A.; Taatjes, C. A. *J. Phys. Chem. A* **1997**, *101*, 1873.

(25) Matsumi, Y.; Izumi, K.; Skorokhodov, V.; Kawasaki, M.; Tanaka, N. *J. Phys. Chem. A* **1997**, *101*, 1216.

(26) Johnston, H. S.; Goldfinger, P. *J. Chem. Phys.* **1962**, *37*, 700.

(27) Chiltz, G.; Goldfinger, P.; Huybrechts, G.; Johnston, H. S.; Meyers, L.; Verbeke, G. *J. Chem. Phys.* **1963**, *38*, 1053.

(28) Truong, T. N.; Truhlar, D. G.; Baldridge, K. K.; Gordon, M. S.; Steckler, R. *J. Chem. Phys.* **1989**, *90*, 7137.

(29) Gonzalez-Lafont, A.; Truong, T. N.; Truhlar, D. G. *J. Chem. Phys.* **1991**, *95*, 8875.

(30) Dobbs, K. D.; Dixon, D. A. *J. Phys. Chem.* **1994**, *98*, 12584.

(31) Duncan, W. T.; Truong, T. N. *J. Chem. Phys.* **1995**, *103*, 9642.

(32) Wang, X.; Ben-Nun, M.; Levine, R. D. *Chem. Phys.* **1995**, *197*, 1.

(33) Espinosa-García, J.; Corchado, J. C. *J. Chem. Phys.* **1996**, *105*, 3517.

(34) Roberto-Neto, O.; Coitiño, E. L.; Truhlar, D. G. *J. Phys. Chem. A* **1998**, *102*, 4568.

(35) Nyman, G.; Yu, H.-G.; Walker, R. B. *J. Chem. Phys.* **1998**, *109*, 5896.

(36) Yu, H.-G.; Nyman, G. *J. Chem. Phys.* **1999**, *110*, 7233.

(37) Yu, H.-G.; Nyman, G. *Phys. Chem. Chem. Phys.* **1999**, *1*, 1181.

(38) Corchado, J. C.; Truhlar, D. G.; Espinosa-García, J. *J. Chem. Phys.* **2000**, *112*, 9375.

(39) Skokov, S.; Bowman, J. M. *J. Chem. Phys.* **2000**, *113*, 4495.

(40) Senkan, S. M.; Robinson, J. M.; Gupta, A. K. *Combust. Flame* **1983**, *49*, 305.

(41) Weissman, M.; Benson, S. W. *Int. J. Chem. Kinet.* **1984**, *16*, 307.

(42) Michelsen, H. A.; Salawitch, R. J.; Gunson, M. R.; Aellig, C.; Kämpfer, N.; Abbas, M. M.; Abrams, M. C.; Brown, T. L.; Chang, A. Y.; Goldman, A.; Irion, F. W.; Newchurch, M. J.; Rinsland, C. P.; Stiller, G. P.; Zander, R. *Geophys. Res. Lett.* **1996**, *23*, 2361.

(43) Tyndall, G. S.; Orlando, J. J.; Kegley-Owen, C. S. *J. Chem. Soc., Faraday Trans.* **1995**, *91*, 3055.

(44) Kandel, S. A.; Zare, R. N. *J. Chem. Phys.* **1998**, *109*, 9719.

(45) Simpson, W. R.; Rakitzis, T. P.; Kandel, S. A.; Orr-Ewing, A. J.; Zare, R. N. *J. Chem. Phys.* **1995**, *103*, 7313.

(46) Simpson, W. R.; Rakitzis, T. P.; Kandel, S. A.; Lev-On, T.; Zare, R. N. *J. Phys. Chem.* **1996**, *100*, 7938.

(47) Hsu, D. S. Y.; Manuccia, T. J. In *Advances in Laser Chemistry*; Zewail, A. H., Ed.; Springer-Verlag: Berlin, 1978; pp 89−92.

(48) Hsu, D. S. Y.; Manuccia, T. J. *Appl. Phys. Lett.* **1978**, *33*, 915.

(49) Manuccia, T. J.; Hsu, D. S. Y. In *Laser-Induced Processes in Molecules*; Kompa, K. L., Smith, S. D., Eds.; Springer: Heidelberg, 1979; pp 270−271.

(50) Vijin, V. V.; Mikheev, A. N.; Petrov, A. K.; Molin, Y. N. *React. Kinet. Catal. Lett.* **1975**, *3*, 79.

(51) Chesnokov, E. N.; Strunin, V. P.; Serdyuk, N. K.; Panfilov, V. N. *React. Kinet. Catal. Lett.* **1975**, *3*, 131.

(52) Rakitzis, T. P.; Kandel, S. A.; Lev-On, T.; Zare, R. N. *J. Chem. Phys.* **1997**, *107*, 9392.

(53) Varley, D. F.; Dagdigian, P. J. *J. Phys. Chem.* **1995**, *99*, 9843.

(54) Rettner, C. T.; Michelsen, H. A.; Auerbach, D. J. *Faraday Discuss.* **1993**, *96*, 17.

(55) Rettner, C. T.; Michelsen, H. A.; Auerbach, D. J. *J. Chem. Phys.* **1995**, *102*, 4625.

(56) Sander, S. P.; Friedl, R. R.; DeMore, W. B.; Golden, D. M.; Kurylo, M. J.; Hampson, R. F.; Huie, R. E.; Moortgat, G. K.; Ravishankara, A. R.; Kolb, C. E.; Molina, M. J. *Chemical Kinetics and Photochemical Data for Use in Stratospheric Modeling*; JPL Publication 00-3; Jet Propulsion Laboratory: Pasadena, CA, 2000.

(57) Atkinson, R.; Baulch, D. L.; Cox, R. A.; Hampson, R. F., Jr.; Kerr, J. A.; Rossi, M. J.; Troe, J. *J. Phys. Chem. Ref. Data* **1999**, *28*, 191.

(58) Lewis, R. S.; Sander, S. P.; Wagner, S.; Watson, R. T. *J. Phys. Chem.* **1980**, *84*, 2009.

(59) Ray, G. W.; Keyser, L. F.; Watson, R. T. *J. Phys. Chem.* **1980**, *84*, 1674.

(60) Dobis, O.; Benson, S. W. *J. Am. Chem. Soc.* **1991**, *113*, 6377.

(61) Kaiser, E. W.; Rimai, L.; Schwab, E.; Lim, E. C. *J. Phys. Chem.* **1992**, *96*, 303.

(62) Stickel, R. E.; Nicovich, J. M.; Wang, S.; Zhao, Z.; Wine, P. H. *J. Phys. Chem.* **1992**, *96*, 9875.

(63) Clyne, M. A. A.; Watson, R. T. *J. Chem. Soc., Faraday Trans. 1* **1974**, *70*, 2250.

(64) Clyne, M. A. A.; Nip, W. S. *J. Chem. Soc., Faraday Trans. 2* **1976**, *72*, 838.

(65) Kurylo, M. J.; Braun, W. *Chem. Phys. Lett.* **1976**, *37*, 232.

(66) Watson, R.; Machado, G.; Fischer, S.; Davis, D. D. *J. Chem. Phys.* **1976**, *65*, 2126.

(67) Zahniser, M. S.; Kaufman, F.; Anderson, J. G. *Chem. Phys. Lett.* **1976**, *37*, 226.

(68) Nicovich, J. M.; Kruetter, K. D.; Wine, P. H. *Int. J. Chem. Kinet.* **1990**, *22*, 399.
(69) Seeley, J. V.; Jayne, J. T.; Molina, M. J. *J. Phys. Chem.* **1996**, *100*, 4019.
(70) Atkinson, R.; Baulch, D. L.; Cox, R. A.; Hampson, R. F., Jr.; Kerr, J. A.; Rossi, M. J.; Troe, J. *IUPAC Subcommittee on Gas Kinetic Data Evaluation for Atmospheric Chemistry*; www.iupac-kinetic.ch.cam.ac.uk, 2000.
(71) (a) Simpson, W. R.; Orr-Ewing, A. J.; Zare, R. N. *Chem. Phys. Lett.* **1993**, *212*, 163. (b) Simpson, W. R.; Orr-Ewing, A. J.; Rakitzis, T. P.; Kandel, S. A.; Zare, R. N. *J. Chem. Phys.* **1995**, *103*, 7299. (c) Orr-Ewing, A. J.; Simpson, W. R.; Rakitzis, T. P.; Kandel, S. A.; Zare, R. N. *J. Chem. Phys.* **1997**, *106*, 5961.
(72) Herzberg, G. *The Spectra and Structures of Simple Free Radicals. An Introduction to Molecular Spectroscopy*; Dover Publications: New York, 1971; p 169.
(73) Bernstein, R. B. *Chemical Dynamics via Molecular Beam and Laser Techniques*; Oxford University Press: New York, 1982; pp 9−12, 20−23.
(74) Wiberg, K. B.; Motell, E. L. *Tetrahedron* **1963**, *19*, 2009.
(75) Wallington, T. J.; Hurley, M. D. *Chem. Phys. Lett.* **1992**, *189*, 437.
(76) Saueressig, G.; Bergamaschi, P.; Cowley, J. N.; Fischer, H.; Harris, G. W. *Geophys. Res. Lett.* **1996**, *23*, 3619.
(77) Tyler, S. C.; Ajie, H. O.; Rice, A. L.; Cicerone, R. J.; Tuazon, E. C. *Geophys. Res. Lett.* **2000**, *27*, 1715.
(78) Saueressig, G.; Bergamaschi, P.; Cowley, J. N.; Fischer, H.; Harris, G. W. *Geophys. Res. Lett.* **1995**, *22*, 1225.
(79) Crowley, J. N.; Saueressig, G.; Bergamaschi, P.; Fischer, H.; Harris, G. W. *Chem. Phys. Lett.* **1999**, *303*, 268.
(80) Berry, R. S.; Rice, S. A.; Ross, J. *Physical Chemistry*, John Wiley and Sons: New York, 1980; pp 1139−1147.
(81) Brown, L. R.; Loete, M.; Hilico, J. C. *J. Mol. Spectrosc.* **1989**, *133*, 273.
(82) Herzberg, G. *Molecular Spectra and Molecular Structure II. Infrared and Raman Spectra of Polyatomic Molecules*; Krieger Publishing Company: Malabar, FL, 1991; pp 306−309.
(83) Aquilanti, V.; Cappelletti, D.; Pirani, F. *J. Chem. Soc., Faraday Trans.* **1993**, *89*, 1467.
(84) Eckart, C. *Phys. Rev.* **1930**, *35*, 1303.
(85) Johnston, H. S.; Heicklen, J. *J. Phys. Chem.* **1962**, *66*, 532. There are several typographical errors in the equations given in this paper. In eq 8, the term $(A^2 - B^2)$ should be squared, and eq 15 should be $2\pi b = 2[(\xi - 1)\alpha_1 + \alpha_2]^{1/2}(\alpha_1^{-1/2} + \alpha_2^{-1/2})^{-1}$.
(86) Chen, Y.; Tshuikow-Roux, E. *J. Phys. Chem.* **1993**, *97*, 3742.
(87) van der Zande, W. J.; Zhang, R.; Zare, R. N.; McKendrick, K. G.; Valentini, J. J. *J. Phys. Chem.* **1991**, *95*, 8205.
(88) Herzberg, G. *Molecular Spectra and Molecular Structure, I. Spectra of Diatomic Molecules*; 2nd ed.; Robert E. Krieger: Malabar, FL, 1989; p 534.
(89) *JANAF Thermochemical Tables*, 2nd ed.; Stull, D. R., Prophet, H., Eds.; National Bureau of Standards: Washington, DC, 1971.
(90) Tan, L. Y.; Winer, A. M.; Pimentel, G. C. *J. Chem. Phys.* **1972**, *57*, 4028.
(91) Frye, J. M.; Sears, T. J.; Leitner, D. *J. Chem. Phys.* **1988**, *88*, 5300.
(92) Parker, D. H.; Wang, Z. W.; Janssen, M. H. M.; Chandler, D. W. *J. Chem. Phys.* **1989**, *90*, 60.
(93) We normalized χ^2 by the number of points N used in the fits (125 for the rate constants and 36 for the KIE), i.e., $\chi^2 = (1/N)\sum[(k - k_i)/\sigma_i]^2$, where k is the fitted value of the rate constant, k_i is the measured value, and σ_i is the estimated (1σ) experimental error.
(94) Michelsen, H. A. *J. Geophys. Res.* **2000**, in press.
(95) Ditchburn, R. W. *Proc. R. Soc.* **1955**, *229A*, 44.
(96) Laufer, A. H.; McNesby, J. R. *J. Chem. Phys.* **1968**, *49*, 2272.
(97) Lee, L. C.; Chiang, C. C. *J. Chem. Phys.* **1983**, *78*, 688.
(98) Slanger, T. G.; Black, G. *J. Chem. Phys.* **1982**, *77*, 2432.
(99) Mordaunt, D. H.; Lambert, I. R.; Morley, G. P.; Ashford, M. N. R.; Dixon, R. N.; Western, C. M.; Schnieder, L.; Welge, K. H. *J. Chem. Phys.* **1993**, *98*, 2054.
(100) Heck, A. J. R.; Zare, R. N.; Chandler, D. W. *J. Chem. Phys.* **1996**, *104*, 4019.
(101) Wang, J.-H.; Liu, K. *J. Chem. Phys.* **1998**, *109*, 7105.
(102) Dessler, A. E.; Considine, D. B.; Morris, G. A.; Schoeberl, M. R.; Russell, J. M., III; Roche, A. E.; Kumer, J. B.; Mergenthaler, J. L.; Waters, J. W.; Gille, J. C.; Yue, G. K. *Geophys. Res. Lett.* **1995**, *22*, 1721.
(103) Rinsland, C. P.; Gunson, M. R.; Salawitch, R. J.; Michelsen, H. A.; Zander, R.; Newchurch, M. J.; Abbas, M. M.; Abrams, M. C.; Manney, G. L.; Chang, A. Y.; Irion, F. W.; Goldman, A.; Mahieu, E. *Geophys. Res. Lett.* **1996**, *23*, 2365.
(104) Zander, R.; Mahieu, E.; Gunson, M. R.; Abrams, M. C.; Chang, A. Y.; Abbas, M.; Aellig, C.; Engel, A.; Goldman, A.; Irion, F. W.; Kämpfer, N.; Michelsen, H. A.; Newchurch, M. J.; Rinsland, C. P.; Salawitch, R. J.; Stiller, G. P.; Toon, G. C. *Geophys. Res. Lett.* **1996**, *23*, 2357.
(105) Stachnik, R. A.; Hardy, J. C.; Tarsala, J. A.; Waters, J. W. *Geophys. Res. Lett.* **1992**, *19*, 1931.
(106) Chance, K.; Traub, W. A.; Johnson, D. G.; Jucks, K. W.; Ciarpallini, P.; Stachnik, R. A.; Salawitch, R. J.; Michelsen, H. A. *J. Geophys. Res.* **1996**, *101*, 9031.
(107) Solomon, S.; Garcia, R. R.; Rowland, F. S.; Wuebbles, D. J. *Nature* **1986**, *321*, 755.
(108) McElroy, M. B.; Salawitch, R. J.; Wofsy, S. C.; Logan, J. A. *Nature* **1986**, *321*, 759.
(109) Molina, M. J.; Tso, T.-L.; Molina, L. T.; Wang, F. C.-Y. *Science* **1987**, *238*, 1253.
(110) Tolbert, M. A.; Rossi, M. J.; Malhotra, R.; Golden, D. M. *Science* **1987**, *238*, 1258.
(111) Webster, C. R.; May, R. D.; Toohey, D. W.; Avallone, L. M.; Anderson, J. G.; Newman, P.; Lait, L.; Schoeberl, M. R.; Elkins, J. W.; Chan, K. R. *Science* **1993**, *261*, 1130.
(112) Molina, L. T.; Molina, M. J. *J. Phys. Chem.* **1987**, *91*, 433.
(113) deZafra, R. L.; Jaramillo, M.; Parrish, A.; Solomon, P. M.; Connor, B.; Barnett, J. *Nature* **1987**, *328*, 408.
(114) Anderson, J. G.; Brune, W. H.; Proffitt, M. H. *J. Geophys. Res.* **1989**, *94*, 11465.
(115) Douglass, A. R.; Schoeberl, M. R.; Stolarski, R. S.; Waters, J. M.; Russell, J. M., III; Roche, A. E.; Massie, S. T. *J. Geophys. Res.* **1995**, *100*, 13967.
(116) Santee, M. L.; Froidevaux, L.; Manney, G. L.; Read, W. G.; Waters, J. W.; Chipperfield, M. P.; Roche, A. E.; Kumer, J. B.; Mergenthaler, J. L.; Russell, J. M., III. *J. Geophys. Res.* **1996**, *101*, 18835.
(117) Grooss, J.-U.; Pierce, R. B.; Crutzen, P. J.; Grose, W. L.; Russell, J. M., III. *J. Geophys. Res.* **1997**, *102*, 13141.
(118) Mickley, L. J.; Abbatt, J. P. D.; Frederick, J. E.; Russell, J. M., III. *J. Geophys. Res.* **1997**, *102*, 21479.
(119) Michelsen, H. A.; Webster, C. R.; Manney, G. L.; Scott, D. C.; Margitan, J. J.; May, R. D.; Irion, F. W.; Gunson, M. R.; Russell, J. M., III; Spivakovsky, C. M. *J. Geophys. Res.* **1999**, *104*, 26419.